EUROfusion

EUROFUSION WPMST1–PR(15)39

W. Zhang et al.

3D Simulations of Gas Puff Effects on Edge Density and ICRF Coupling in ASDEX Upgrade

Preprint of Paper to be submitted for publication in
Nuclear Fusion

This work has been carried out within the framework of the EUROfusion Consortium and has received funding from the Euratom research and training programme 2014-2018 under grant agreement No 633053. The views and opinions expressed herein do not necessarily reflect those of the European Commission.

3D simulations of gas puff effects on edge density and ICRF coupling in ASDEX Upgrade

W. Zhang[1,2,3,a)], V. Bobkov[2], T. Lunt[2], J-M. Noterdaeme[1,2], D. Coster[2], R. Bilato[2], P. Jacquet[4], D. Brida[2], Y. Feng[2], E. Wolfrum[2], L. Guimarais[5] and the ASDEX Upgrade Team[2]

[1]*Applied Physics Department, University of Ghent, Ghent, Belgium*

[2]*Max-Planck-Institut für Plasmaphysik, Garching/Greifswald, Germany*

[3]*Institute of Plasma Physics, Chinese Academy of Sciences, Hefei, P. R. China*

[4]*CCFE, Culham Science Centre, Abingdon, UK*

[5]*Instituto de Plasmas e Fusão Nuclear, IST, Universidade de Lisboa, Portugal*

[a)]Corresponding author: wei.zhang@ipp.mpg.de

Abstract.

In recent experiments, a local gas puff was found to be an effective way to tailor the Scrape-Off Layer (SOL) density and improve the Ion Cyclotron Range of Frequency (ICRF) power coupling in tokamaks. In order to quantitatively reproduce these experiments, to understand the corresponding physics and to optimize the gas valve positions and rates, simulations were carried out with the 3D edge plasma transport code EMC3-EIRENE in ASDEX Upgrade. An inter-ELM phase of an H-mode discharge with a moderate gas puff rate (1.2×10^{22} electrons/s) is used in our simulations. We simulated cases with gas puff in the lower divertor, the outer mid-plane and the top of the machine while keeping other conditions the same. Compared with the lower divertor gas puff, the outer mid-plane gas puff can increase the local density in front of the antennas most effectively, while a toroidally uniform but significantly smaller enhancement is found for the top gas puff. Good agreement between our simulations and experiments is obtained. With further simulations, the mechanisms of SOL density tailoring via local gas puffing and the strategies of gas puff optimization are discussed in the paper.

1. Introduction

Plasma heating in the Ion Cyclotron Range of Frequencies (ICRF) is one of the main auxiliary plasma heating methods in tokamaks. It relies on the Fast Wave (FW) to transport the power from the plasma edge where the antenna is located to the plasma center. Since the FW is evanescent below the cut-off density (typically in the 10^{18} m^{-3} range), the wave decays rapidly in the region where the density is below this value in the Scrape-Off Layer

(SOL). The coupling depends strongly on the width of this evanescence region. To a first approximation, the coupled ICRF power can be described by $P_{coupled} \sim V_{max}^2 R_c / 2Z_c^2$, where V_{max} is the anti-node voltage in the transmission line and Z_c is the transmission line characteristic impedance. The coupling resistance R_c depends exponentially on the evanescence distance between the ICRF antenna and FW cut-off layer, i.e. $R_c \propto R_0 e^{-\alpha \cdot R_{evan}}$, where α is the tunneling factor [1]. This evanescence distance can be made smaller by increasing the edge density in front of the ICRF antennas.

Previous experiments in ASDEX Upgrade (AUG) [2, 3], JET [4, 5] and DIII-D [6, 7] show that the edge density can indeed be increased by using top or outer mid-plane deuterium gas injected close to the antennas instead of divertor gas. An increase by a factor two of antenna loading in these tokamaks was reported for the antennas close to the outer mid-plane valves in [8]. Encouraged by these experiments, maximization of ICRF power by optimizing the gas valve positions and rates is considered in several present and future tokamaks, such as AUG, JET, DIII-D, EAST, WEST and ITER.

In order to quantitatively reproduce the previous experiments, optimize the spatial location of the valves and predict the required amounts of gas, numerical simulations are required. Due to the assumption of toroidal axisymmetry, 2D codes such as EDGE2D-EIRENE cannot quantitatively reproduce the experimental results [8]. In contrast to that, EMC3-Eirene is a coupled Edge Monte Carlo 3D plasma fluid (EMC3) [9] and kinetic neutral particle (Eirene) [10] code. The 3D nature of the code makes it particularly suitable for studying the 3D physics such as gas puff effects on ICRF power coupling. By including the toroidal nonaxisymmetrical Plasma Facing Components (PFCs) and the gas valves at the correct 3D positions, the simulations can be made more realistic. We report the simulation results on an inter-ELM phase of an H-mode discharge with different gas puff locations in AUG. Once the model is validated against experiments, it could be applied to ITER and other future fusion devices in order to predict the optimum gas valve positions and gas puff rate for maximized ICRF power coupling.

In this paper, the simulation setups and validation with experiments are described in Section 2. In section 3, the main simulation results are discussed in detail. The mechanisms of how the local gas puff influences the SOL density are presented in section 4. The strategies for optimizing the gas puff are discussed in setion 5. Finally conclusions and an outlook are given in section 6.

2. Simulation setups

EMC3-Eirene was originally developed for W7-AS and is now a standard modelling code for helical devices. It has also been widely applied to various tokamaks including ITER [11]. The interest in 3D simulation of the SOL in tokamaks is triggered by the 3D effects of Resonant Magnetic Perturbation (RMP) fields [12, 13], the local gas puff [14] and the 3D particle and energy flow to the main chamber wall [15]. This paper will discuss in detail the implemention of the code in the gas puff studies.

The AUG discharges (table 1) in our study are type-I ELMy H-modes with B_t=2.5T, I_p=0.8MA, P_{total}=7.8MW (P_{ICRF}=1.5MW at 36.5MH) and total radiated power $P_{radiated}$=3.2MW. The deuterium gas puff rate in the time period [1.3, 3.0s] and [5.0, 7.0s] for all discharges are the same (1.2×10^{22} el/s). Different gas puff methods are investigated in these discharges.

To carry out comprehensive simulations with EMC3-Eirene, a computation grid covering 360° was built and implemented in our simulations. The equilibrium, calculated by CLISTE [16], is from discharge 31269 at 2.1s. Figure 1 illustrates the poloidal cross-section of the computation grid at Φ=11.25^o. Both EMC3 and Eirene share the same grid including the outer core (in red color), the Scrape-Off Layer (SOL) (in blue and green color) and the Private Flux Region (PFR) (in cyan color). The SOL region of the computation grid is extended to the main chamber wall with a part (in green color) which does not necessarily have to be flux surface aligned. The region inside the vessel and outside the SOL (in yellow color) is used only by Eirene. Figure 2 shows the 3D structure of the grid on a flux surface in the SOL. The full 360° grid is composed of sixteen equally constructed segments. Each segment has a toroidal angle of 22.5^o and represents a sector in AUG. The PFCs in our computation model include the upper and lower divertors, the inner heat shield, four auxiliary limiters and eight ICRF antenna limiters. For the convenience of calculations, the toroidal angle is counted from -180° to 180°, and the 0° position is chosen at the boundaries of sector 5 and sector 6 (Figure 3). In our simulations no impurities are considered, hence the radiated power is subtracted from the total power to approximate the total power deposited on the PFCs by the plasma. The separatrix electron density is about 2.5×10^{19} m^{-3} and is used as a boundary condition in EMC3-Eirene. The gas puff rate (1.2×10^{22} el/s) in the code was set to be equal to 6% of the total recycling flux, and the rest 94% is treated as the amount of the recyling flux from the main chamber wall and the divertors. By this setting the total particles in our model are kept balanced, and no gas pump was considered in these simulations.

An ELMy H-mode plasmas (#31269 at 2.1s) with lower divertor gas puff rate 1.2×10^{22} el/s was firstly simulated. The density (n_e) and temperature (T_e) profiles in the mid-plane and the ion saturation current density (j_{sat}) in the divertor are fitted to the experiments by modifying the tranport parameters (i. e. particle and heat diffusion coefficient $D_\perp$ and $\chi_\perp$, respectively) in the code. The diagnostics used in the comparisons include the Lithum beam for n_e [17], the edge and core Thomson scattering for n_e and T_e [18], and the divertor Langmuir probes for j_{sat} [19]. Only the inter-ELM experimental data is used, because the inter-ELM phases are those of interest corresponding to the lowest coupling resistance and maximum antenna voltages [8]. The transport parameters are chosen such that the final n_e, T_e and j_{sat} profiles in our simulations agree well with the experiments (Figure 4), except for the j_{sat} values at the inner strike point.

After validating our simulations with experiments for the lower divertor gas puff case, the gas sources are then switched to the top or the outer mid-plane of the vessel to study the related changes in the 3D distribution of n_e and T_e. For experiments in AUG, usually 4 gas valves are used for the lower divertor gas puff, and one for each top or outer mid-plane gas puff. The following cases (table 2) were simulated in parallel with the experiments (table 1): I. four lower divertor gas valves in sectors 1, 5, 9, 13 (toroidal angle Φ=-101.25^o, -11.25^o, 78.75^o, 168.75^o); II. one top gas valve in sector 2 (Φ=-78.75^o); III. one top gas valve in sector 7 (Φ=33.75^o); IV. one outer mid-plane gas valve in sector 3 (Φ=-56.25^o); V. one outer mid-plane gas valve in sector 13 (Φ=168.75^o). The total gas puff rate in all cases is the same (1.2×10^{22}el/s).

3. Simulation results

3.1 Gas puff effects on edge density

Poloidal cross-sections of the neutral atom densities during the lower divertor, the top and the outer mid-plane gas puff are shown in the upper row of Figure 5. Toroidal positions are chosen where the gas valves are placed, so the poloidal cross-sections are the same either for the top gas puff case II (Φ=-78.75^o) and case III ((Φ=33.75^o), or for the outer mid-plane gas puff case IV (Φ=-56.25^o) and case V ((Φ=168.75^o). The arrows in the figure are used to represent the positions and directions of the injected gas. A localized cloud of neutrals near the valves could be seen both in the top and the lower divertor gas puff cases. For the outer mid-plane gas puff, the poloidal and toroidal distribution of the enhanced neutral density essentially corresponds to the shape of the so-called A-port. The corresponding electron densities are depicted in the lower row of Figure 5. The radial and poloidal localization of the electron density near the top gas valve (Figure 5, second column) can be explained by the fact that the gas is ionized locally in the SOL and the particle transport in the parallel direction of the magnetic field is much larger than in the perpendicular. For the outer mid-plane gas puff, the density is enhanced in a large poloidal range in the outer mid-plane. The striped density structures in the top of the SOL are consequences of helical paths in which magnetic field lines connect the mid-plane and top (Figure 5, third column).

Note that the outer mid-plane gas valves are located very deep in the A-port in AUG. Before the gas reaches the plasma edge, it has already spread widely and becomes an almost homogeneous source in the cross-section of the port. The scattered gas is firstly shaped by the front face of the port and then by the PFCs such as the limiters. In the simulations, we have put the mid-plane gas valves as far as possible to the edge of the computational grid. In that way the gas fills-up the A-port. This gives a realistic description of the ionization area where neutrals interact with the plasma. Figure 6 shows the electron density comparisons between the EMC3-Eirene simulations and reflectometer measurement in sector 5 (~ 1.73m away from the A03 mid-plane valve, Figure 3). For the reflectometer data (#30634), only densities in the range [0.3×10^{19}, 1.5×10^{19} m^{-3}] are accurate, and those below 0.3×10^{19} m^{-3} are extrapolated. Good agreement is found for the lower divertor gas puff (case I), while only a small discrepancy in the density range [0.4×10^{19}, 0.85×10^{19} m^{-3}] is seen for the A03 mid-plane gas puff (case IV). This shows that the physical description of the outer mid-plane valve in EMC3-Eirene is reasonable.

To investigate the edge density distributions in the toroidal direction, toroidal cross-sections in the outer mid-plane (Z=0.0m) are made for the cases I, II, IV and V (Figure 7). Only densities larger than the cut-off density (~4×10^{18} m^{-3}) are shown in the plot. The position of the cut-off density for case I (the horizontal dashed line) is used as a reference. The results indicate that the edge density is increased toroidal uniformly by a small margin with the top gas puff, while the density near the valves can be notably increased with the outer mid-plane gas puff. This density increase significantly reduces the width of the evanescent layer. For the density in the region far away from the outer mid-plane valve, no obvious change can be seen.

Furthermore, we calculated the averaged electron density in front of each ICRF antenna. This average is made both in the poloidal and toroidal directions covering the whole range of the antenna, namely

$$\langle n_e(\psi)\rangle = \frac{1}{\Delta\theta\Delta\Phi}\int_{\theta_0-\Delta\theta/2}^{\theta_0+\Delta\theta/2}\int_{\Phi_0-\Delta\Phi/2}^{\Phi_0+\Delta\Phi/2} n_e(\psi,\theta,\Phi)\,d\theta\, d\Phi$$

in which θ_0 and Φ_0 represent the poloidal and toroidal angles of the antenna center, and $\Delta\theta$ and $\Delta\Phi$ are the angles between the edges of the antennas in the poloidal and toroidal directions respectively. The averaged density

in each flux surface $\langle n_e(\psi)\rangle$ is then transformed to $\langle n_e(R)\rangle$ at Z=0.0m. The results are shown in Figure 8. In each subplot, the dashed line represents the averaged density profile during the lower divertor gas puff (case I), and the dash-dotted lines is the cut-off density of the ICRF FW. From the analysis we find that the top gas puff can increase the edge density only to a small extent. However, this increase is toroidally uniform and independent of the toroidal positions of the gas valve (Figure 8 (a) and (b)). The outer mid-plane gas puff can significantly increase the edge density in the area near the valve. In the case IV, the gas valve is located between antenna 1 and 2 (closer to antenna 2) and far away from antenna 3 and 4, thus the density is enhanced largely in front of antennas 1 and 2, while almost no change is observed for antennas 3 and 4 (Figure 8 (c)). In the case V, the toroidal distance from the valve to the antennas 4, 3, 1, 2 is increasing, and the density enhancement has the inverse trend, i.e. the largest density increase is seen for antenna 4 and the smallest for antenna 2 (Figure 8 (d)). The top gas puff (cases II or III) can reduce the evanescence distance by ~0.73cm, while the outer mid-plane gas puff can have a larger effect, such as case IV can make this distance smaller by ~1.96cm. Based on these results and further calculations with FELICE [20], the coupling resistances can be calculated.

3.2 Gas puff effects on ICRF power coupling

As mentioned in the introduction, to a first approximation the coupled ICRF power is proportional to the coupling resistance R_c. The relative coupling resistance R_c/R_{c0} both from experiments and combined EMC3-Eirene and FELICE simulations are shown in Figure 7. R_{c0} is the resistance for the lower divertor gas puff (case I) and is used as a reference. The philosophy of calculating the resistance in our simulation is that, firstly the 3D edge density and temperature profiles from EMC3-Eirene are averaged into 1D for each antenna. Then by combining these 1D edge profiles with the experimental core profiles, inputs could be provided to the 1D code FELICE which calculates R_c [21].

According to both the simulations and the experimental antenna resistance database, the top gas puff can improve R_c by 20%~30%, while the outer mid-plane gas puff can increase R_c more remarkably, especially for antennas near the gas valves. A coupling improvement of more than 100% with the outer mid-plane gas puff is observed in experiments for antenna 1 and 2 during A03 puffing (case IV) and for antenna 4 during A13 puffing (case V). The R_c/R_{c0} from the EMC3-Eirene/FELICE simulations and experiments agree well for case II. For case III and V the correct trend is simulated, but the calculated values are consistently lower than the experimental ones. Various mechanisms may be responsible for the larger off-set observed for the outer mid-plane gas puff cases:

1. Consequence of the 1D averaging of the 3D data from EMC3-Eirene. With this averaging method the poloidal and toroidal inhomogeneity of the density in front of the antennas are neglected, and inaccuracies can then be introduced. Taking the A03 mid-plane puff (case IV) for example, the 1D density profile (Figure 8) shows the cut-off density layer is at R=2.192m in front of antenna 1. However the toroidal cross section of the density (Figure 7) implies that this cut-off layer could reach R=2.195m for the same antenna. This averaging method can cause the resistances from the combined simulations to be lower than the experimental ones. For the top gas puff, because the density is enhanced toroidal uniformly, thus the averaging does not have much effects.

2. In our simulations, we do not consider the interactions between the ICRF waves with the plasma. Large inhomogeneous rectified potentials and ponderomotive effects can be induced in front of antennas, resulting in significant convective transport in the plasma edge [22, 23]. This convective transport will cause local density modifications and ultimately influence the coupling resistance.
3. The ELMs can change the SOL properties, even if they are filtered out in our calculations by removing the data in a time window coincident with each ELM event.

Our combined EMC3-Eirene/FELICE simulations confirm that the outer mid-plane gas valves are the most effective in improving the coupling by changing the SOL density. However, for enhancing the agreement with experiments and therefore the predictive capabilities of the simulations, several improvements of the simulations are foreseen for the near future: 1. Using the 2D code TOPICA instead of the 1D code FELICE for resistance calculations. 2. Taking the convective transport caused by the edge ICRF fields into account. 3. Including more detailed structures behind the limiters.

4. Mechanisms of influence of local gas puff on density in the SOL

Different gas puff methods, i.e. gas puffing from the top, outer mid-plane or bottom (the lower divertor) of the machine, can lead to different edge density profiles. Our studies indicate that this is mainly due to the magnetic connections to the ion density cloud in front of the gas valves. A cloud of neutrals puffed at the plasma edge leads to the formation of a plasma density cloud due to ionization (Figure 5). The charged particles in the cloud will strongly follow the magnetic field lines, since from the fluid plasma consideration, the velocities parallel to the magnetic field lines are much larger than the crossing field ones. Thus on the same flux surface, electron densities in the regions which are magnetically connected to the plasma density cloud would be higher than those without.

This is shown by tracing the magnetic field lines from the plasma density cloud in front of the valves (Figure 9 and 10). Four vertical points within the cloud are chosen for the field line tracings. For the top gas puff, field lines encounter a large toroidal spread from the top toward the outer-mid-plane which explains the evenly toroidally distributed density at the outer mid-plane (Figure 9). For the outer mid-plane gas puff, field lines start from the mid-plane have little divergency in a large toroidal range [200°, 400°] when they travel to the top or lower divertor (Figure 10). The magnetic field lines penetrating the plasma density cloud would also pass in front of antennas 1 and 2, resulting in significantly increased electron density there. Thus, gas valves which can generate a homogenous density cloud covering the height of the antennas and being magnetically connected to the antennas are prefered.

5. Strategies for gas puff optimization

Gas puffing at the outer mid-plane of the vessel is indicated to be the most effective in improving the ICRF coupling. When applying this method, one needs to consider the particle and power fluxes to the main chamber wall. As shown in Figure 11, if the outer mid-plane gas valve is put too close to the limiter, a large density bump would occur in the plasma edge. This can cause significant particle flows to the PFCs and large amounts of impurities might be sputtered. The denstity bump can be eliminated by radially shifting the gas valve outward. The more radially retracted the gas valve is, the more poloidally homogenous the electron density would be. During the

shifting process (Figure 11), the coupling is found not decreased as long as the plasma density cloud is within the height of the antennas. To generate a homogenous density cloud covering the antenna, one can also use poloidally distributed gas valves. For example in AUG, 11 poloidally distributed gas valves behind the left limiter of antenna 3 are being installed to improve the coupling of the nearby antennas.

Besides the valve positions, the gas puff rate Φ_{D2} has also an important impact on the coupling. To understand the relationship between Φ_{D2} and the coupling, simulations are carried out for the A03 mid-plane gas puff (case IV) with different Φ_{D2}. Combined EMC3-Eirene and FELICE simulations are used to calculate the relative coupling resistance R_c/R_{c0}. The results (Figure 12) indicate that R_c/R_{c0} could be increased simply by increasing Φ_{D2}. However this does not mean that the higher Φ_{D2} the better, since a strong gas puff can degrade the plasma confinement [24]. In addition, the relative increase of R_c/R_{c0} would become smaller when Φ_{D2} is larger. For instance R_c/R_{c0} increases almost linearly for Φ_{D2} in the range A=[0, 1.5×10^{22} el/s] and B=[1.9×10^{22}, 3.5×10^{22} el/s], but the slope of Φ_{D2} in the range A (k_A) is much larger than the one in the range B (k_B). For antenna 1, k_A ~0.478, k_B ~0.138, and for antenna 2, k_A ~ 0.526, k_B ~0.119. From the economical view, gas puffing with Φ_{D2} in the range [1.2×10^{22}, 1.9×10^{22} el/s] can achieve a high coupling resistance most effectively.

6. Conclusions and Outlooks

For the first time EMC3-Eirene simulations for AUG with a full 360° grid including the main chamber PFCs, divertors and 3D gas puffs were carried out. Our simulation results are in quantitative agreement with the experiment: The top gas puff can increase the edge density uniformly in toroidal direction to a small extent, independent of the toroidal position of the top valves. For the outer mid-plane gas puff the enhancement of the edge density is most significant near the valve and decreases gradually in the toroidal direction; the largest increase is found in front of the antenna nearest to the valve, and almost no change is observed for the antennas far away. Our study indicates that the connection between the cloud of enhanced plasma density and the antennas along magnetic field lines is the reason for the density enhacement in front of the antennas. The plasma density cloud is generated from the ionization of the injected gas near the valves. Thus for ICRF coupling purposes, if poloidal localization of the density increase is not problematic, poloidally distributed gas valves (covering the height of the antennas) which are close to the ICRF antennas in the toroidal direction is the better option.

In the near future we will have better comparison with experiments as more toroidal distributed reflectometers are being installed in AUG. Further EMC3-Eirene simulations and comparisons with experiments in L and H mode discharges in AUG will allow optimization of the gas valve positions in AUG for the purpose of ICRF power coupling and reliable benchmarking of the 3D code in view of its use for ITER. We plan to carry out similar simulations for JET and ITER including the divertor/PFCs/gas valves configurations in full 360° geometry.

Acknowledgments: This work has been carried out within the framework of the EUROfusion Consortium and has received funding from the Euratom research and training programme 2014-2018 under grant agreement No 633053. The views and opinions expressed herein do not necessarily reflect those of the European Commission.

[1] Bilato R. et al 2005 Nucl. Fusion 45 L5–7
[2] Jacquet P. et al 2012 Nuclear Fusion 52 042002
[3] Bobkov V. et al 2014 AIP Conf. Proc. 1580, 271
[4] Lerche E. et al 2014 J. Nucl. Mater. http://dx.doi.org/10.1016/j.jnucmat.2014.10.074 in press
[5] Mayoral M.-L. et al 2007 AIP Conf Proc. 933 p.55
[6] Pinsker R.I. et al 2011 37th EPS Conf. http://ocs.ciemat.es/EPS2010PAP/pdf/O4.124.pdf
[7] Pinsker R.I. et al 2011 AIP Conf Proc. 1406 p.313
[8] Jacquet P. et al 2014 Proc. 25th Int. Conf. on Fusion Energy (St. Petersburg, Russia, 2014), EX/P5-39
[9] Feng Y. et al 2004 Contrib. Plasma Phys. 44 No. 1-3, 57-69
[10] Reiter D. et al2005Fusion Sci. Technol.47 172–86
[11] Feng Y. et al 2014 Contrib. Plasma Phys. 54 No. 4-6, 426 – 431
[12] Frerichs H. et al 2010 Nucl. Fusion50 034004
[13] Lunt T. et al 2012 Nucl. Fusion 52 054013
[14] Zhang W. et al 2015 21st RF Topical Conf. RF Power in Plasmas A56
[15] Lunt T. et al 2015 J. Nucl. Mater. 463 744–747
[16] McCarthy P.J. 1999 Phys. Plasmas 6 3554
[17] Fischer R. et al 2008 Plasma Phys. Control. Fusion 50 085009
[18] Kurzan B. et al 2011 Rev. Sci. Instrum. 82 103501
[19] M. Weinlich et al 1996 Contrib. Plasma Phys. 36 S 53-60.
[20] Brambilla M. et al 1995 Nucl. Fusion 35 1265-1280
[21] Bobkov V. et al 2015 21st RF Topical Conf. RF Power in Plasmas A44
[22] Colas L. et al 2007 Plasma Phys. Control. Fusion49 B35–B45
[23] Eester D.-V. et al 2013 Plasma Phys. Control. Fusion 55 025002
[24] Kalupin D. et al 2001 Plasma Phys. Control. Fusion 43 945–957

		#30634	#30636	#31269	#31273
Gas valve positions	1.3-3.0s	Lower divertor puff	Lower divertor puff	Lower divertor puff	A13 mid-plane puff
	5.0-7.0s	A03 mid-plane puff	A02 top puff	A07 top puff	A10 top puff
Common parameters		ELMy H-mode, $H_{98}(y,2)\approx 0.95$ Gas puff rate (1.2×10^{22}el/s) B_t=2.5T, I_p=0.8MA, P_{total}=7.8MW, P_{radtot}=3.2MW P_{ICRF}=1.5MW, f_{ICRF}=36.5MH, $n_{e,cutoff}$= 0.4×10^{19} m^{-3}			

Table 1. The main parameters of the AUG discharges considered.

Simulated cases	Valve positions (toroidal)	Gas puff rate
case I (lower divertor puff)	sector 1 (Φ=-101.25^o), sector 5 (-11.25^o) sector 9 (78.75^o), sector 13 (168.75^o)	0.3×10^{22}el/s for each valve
case II (A02 top puff)	sector 2 (Φ=-78.75^o)	1.2×10^{22}el/s
case III (A07 top puff)	sector 7 (Φ=33.75^o)	1.2×10^{22}el/s
case IV (A03 outer mid-plane puff)	sector 3(Φ=-56.25^o)	1.2×10^{22}el/s
case V (A13 outer mid-plane puff)	sector 13 (Φ=168.75^o)	1.2×10^{22}el/s

Table 2. The simulated cases in parallel with the experiments.

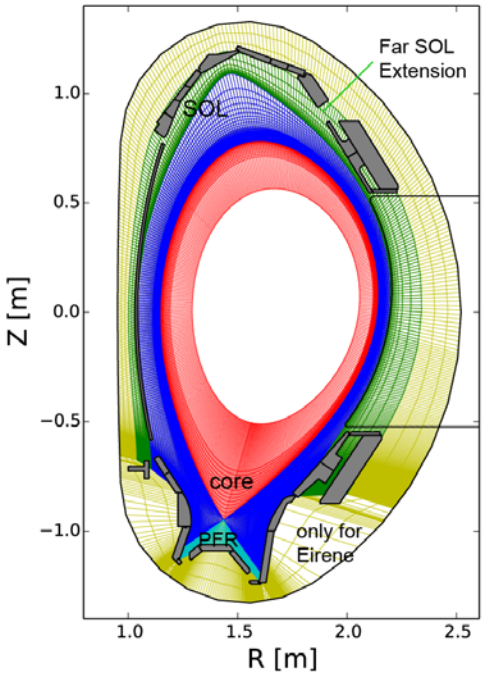

Figure 1. Poloidal cross-section of the computation grid at Φ=11.25^{o}. The SOL region (in blue and green color) of the grid is extended to the main chamber wall. The plasma facing components include the lower and upper divertors, the inner hear shield and sixteen limiters.

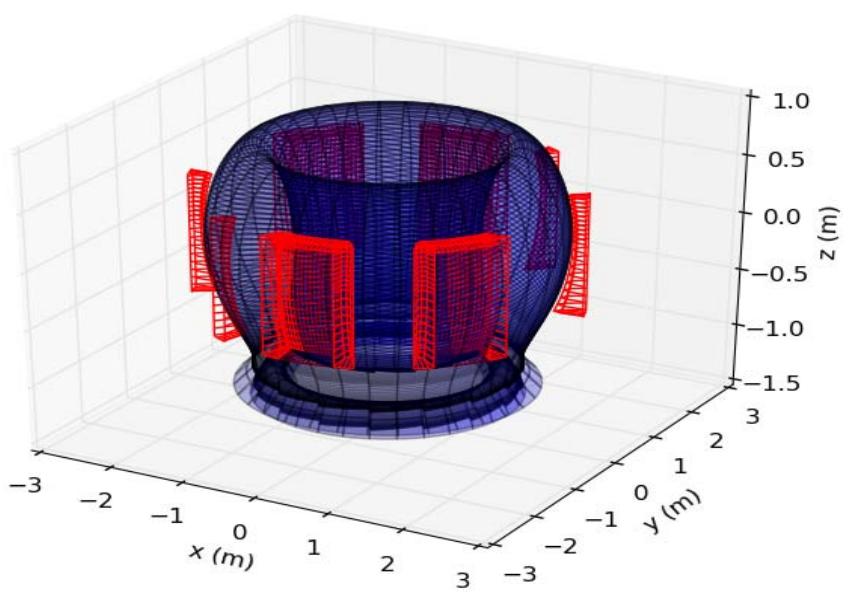

Figure 2. The 3D grid with 8 limiters (two on both sides of each ICRF antenna) and 4 auxiliary limiters.

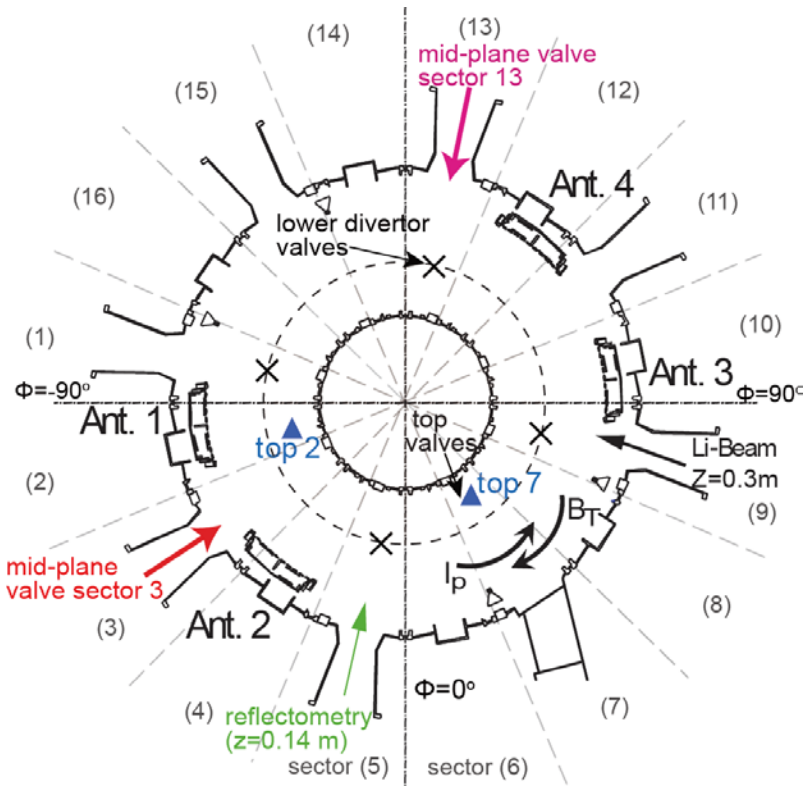

Figure 3. Top view of AUG illustrates the toroidal positions of the ICRF antennas and gas valves.

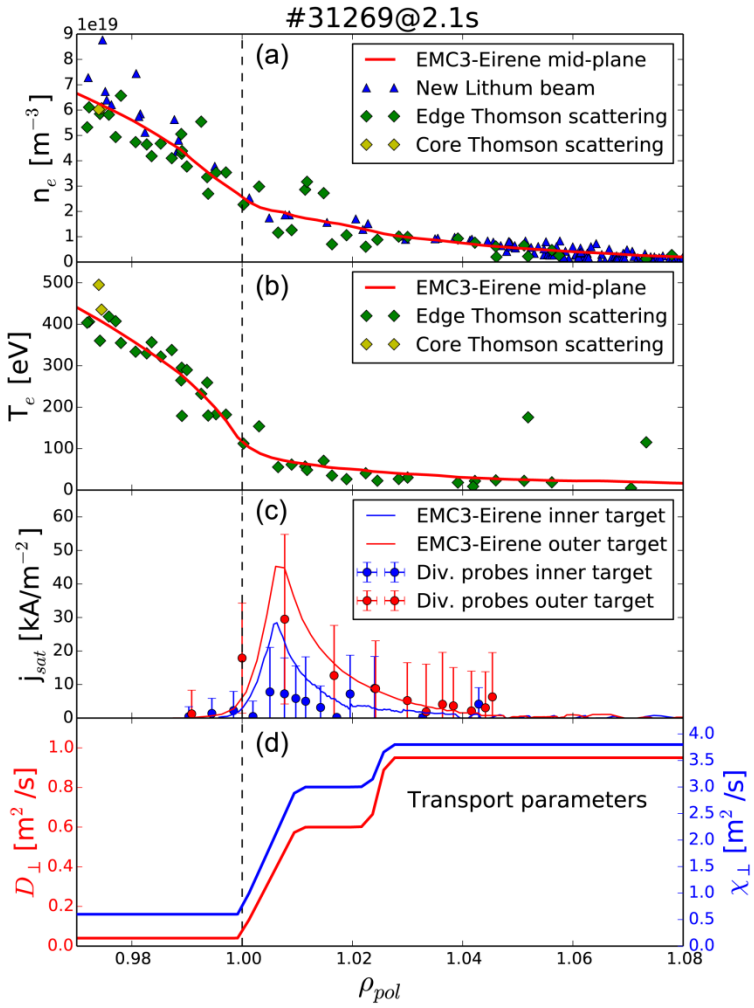

Figure 4. EMC3-Eirene simulations compared with experimental diagnostics for the lower divertor gas puff (case I). (a) Comparisons of mid-plane density profile. (b) Comparisons of mid-plane temperature profile. (c) Comparisons of the ion saturation current density in the targets. (d) Transport parameters $D_\perp$ and $\chi_\perp$ in the code.

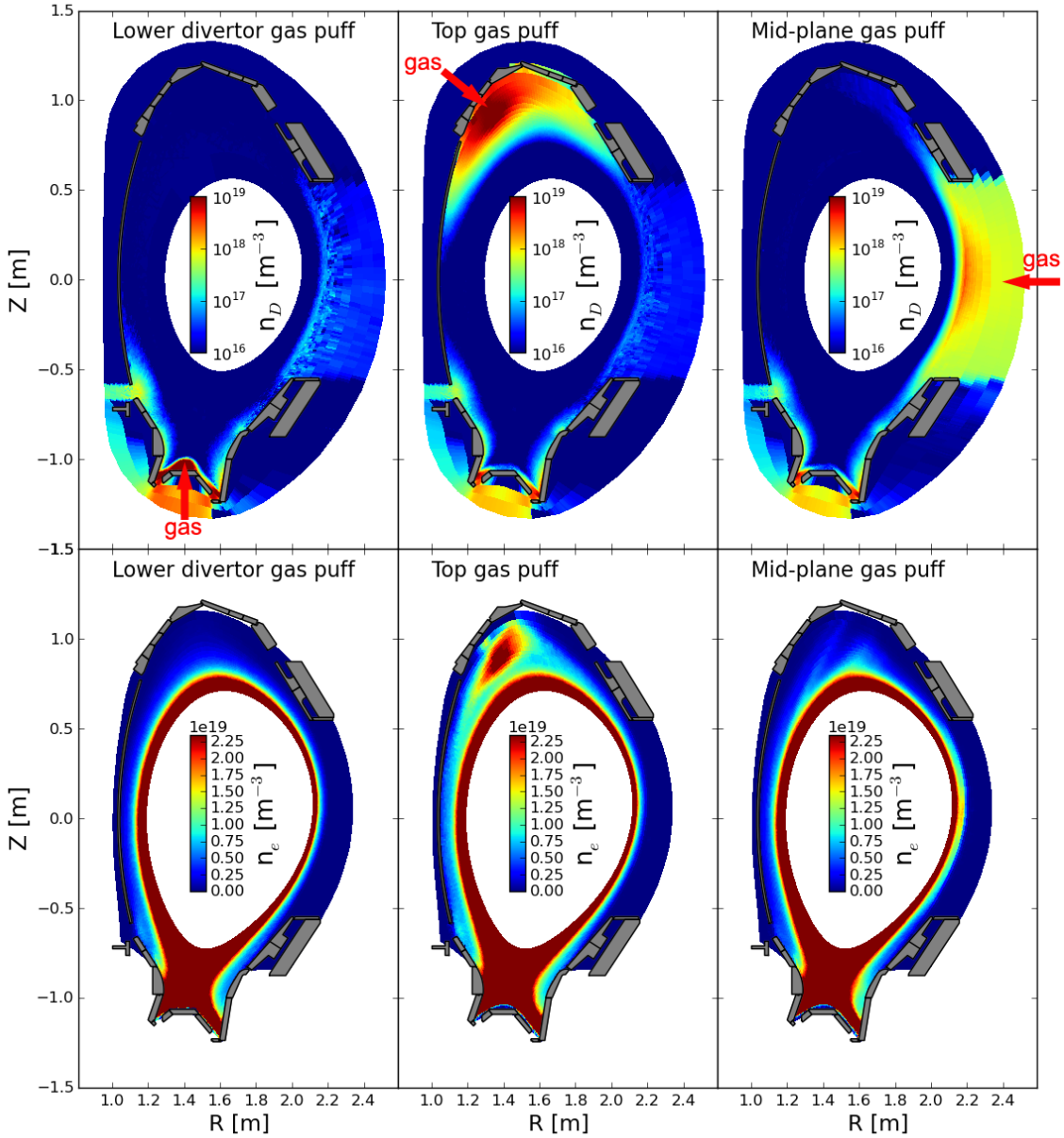

Figure 5. Poloidal cross sections of the neutral atom and electron densities for the lower divertor, top and outer mid-plane gas puff cases. In all cases the gas puff rate is the same. The cross-sections are the same either for the top gas puff case II (Φ=-78.75^o) and case III (Φ= 33.75^o), or for the outer mid-plane gas puff case IV (Φ= -56.25^o) and case V (Φ=168.75^o).

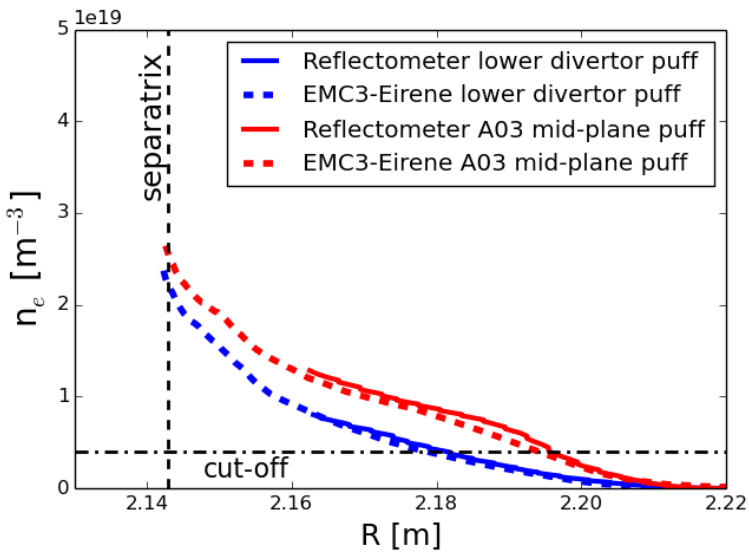

Figure 6. Density comparisons with the reflectometer measurement in sector 5 for the lower divertor gas puff (case I) and the A03 mid-plane gas puff (case IV). The reflectometer profiles (#30634) are averaged over time period 2.1-2.3s (the lower divertor puff) and 5.9-6.1s (the A03 mid-plane puff) respectively. Only the inter-ELM reflectometer data is used.

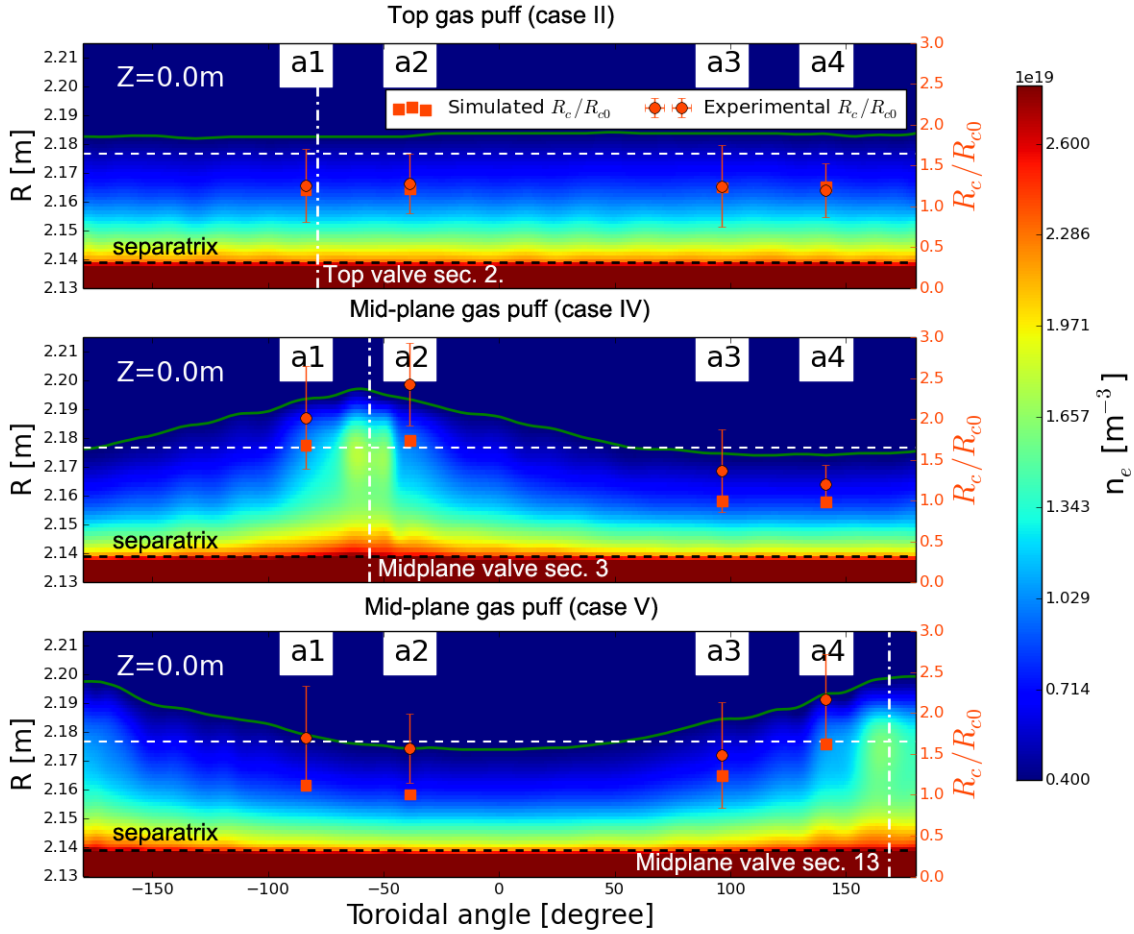

Figure 7. Toroidal cross sections (at Z=0.0m) of the electron density for cases II, IV and V. In each subplot, the green line represents the position of the cut-off density, while the horizontal dashed line represents this position for case I. The vertical dash-dotted line means the toroidal angle of the gas valve. Also shown in the figure are the relative resistances from the experiments and combined EMC3-Eirene and FELICE simulations, the ordinate axises (R_c/R_{c0}) are given in the right side of the figure.

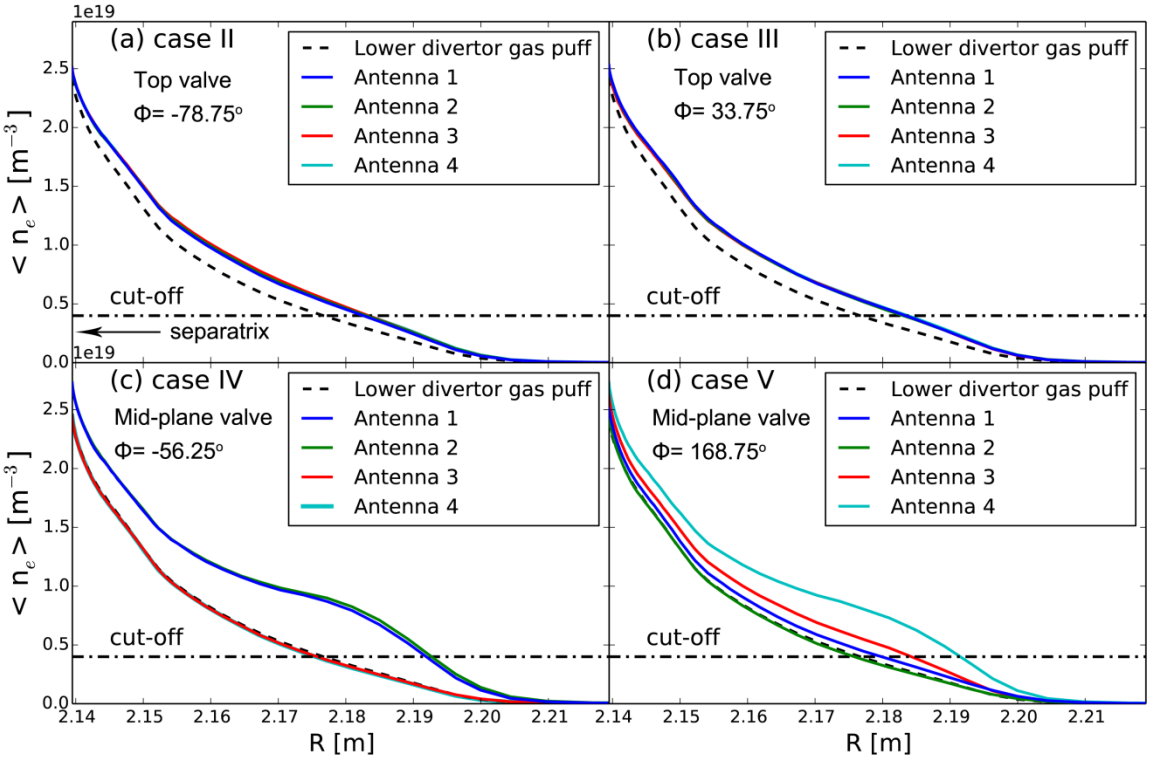

Figure 8. Comparisions of the averaged densities in front of the four antennas for the top gas puff (case II, III) and the outer mid-plane gas puff (case IV, IV). In each subplot, the dashed line represents the density profile in the lower divertor gas puff (case I).

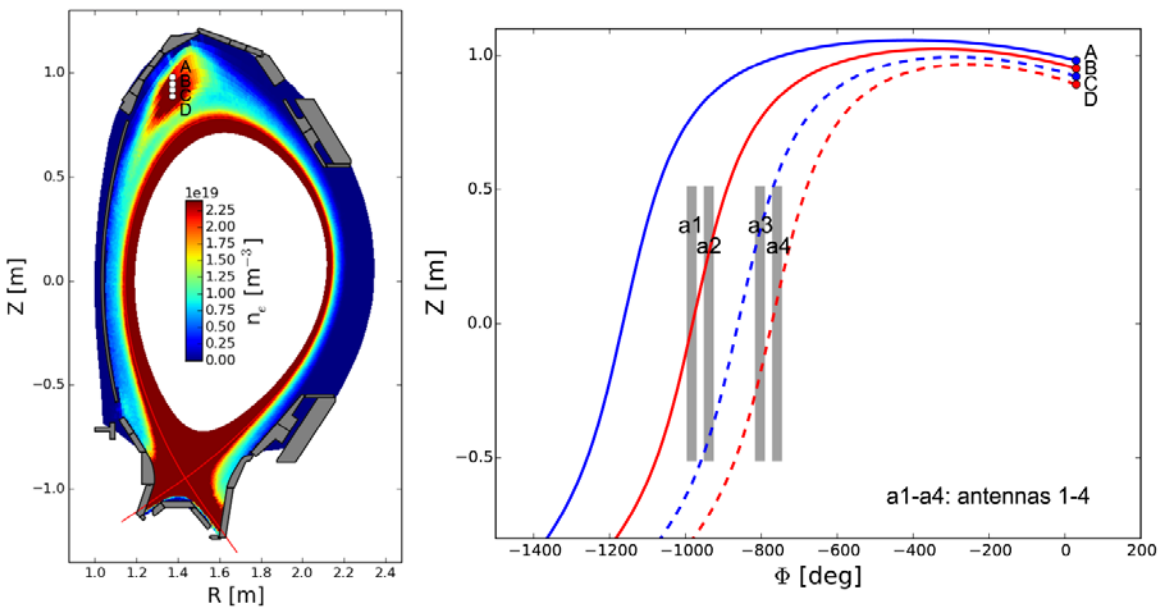

Figure 9. Field lines tracing from the top. The starting points A, B, C, D (in a vertical line) are within the plasma density cloud in front of the top valve.

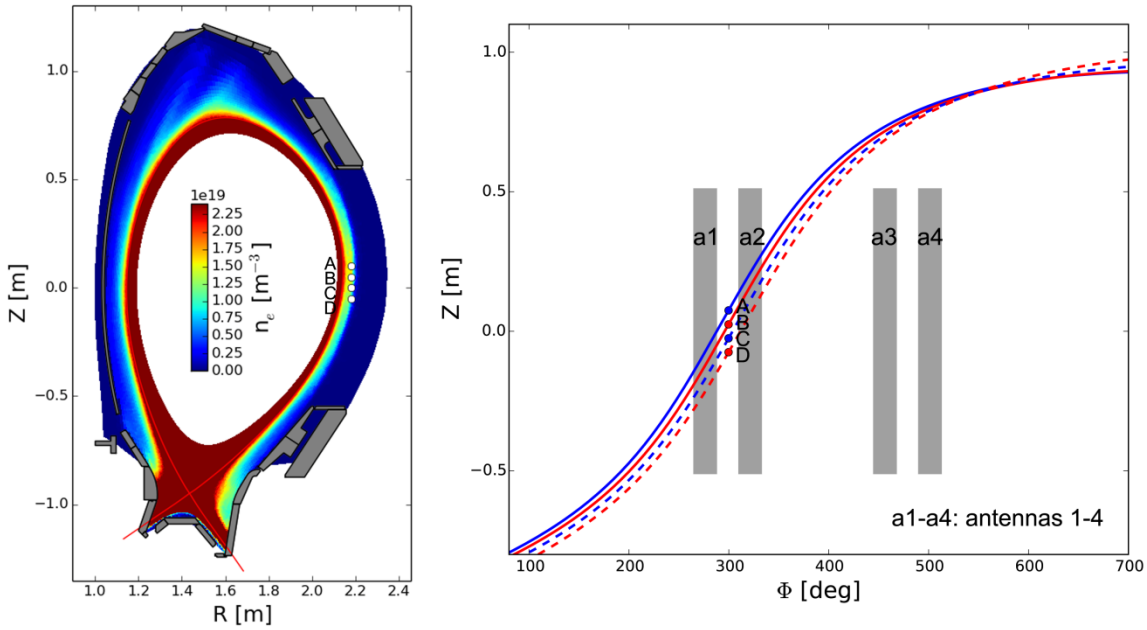

Figure 10. Field lines tracing from the outer mid-plane. The starting points A, B, C, D (in a vertical line) are within the plasma density cloud in front of the outer mid-plane valve.

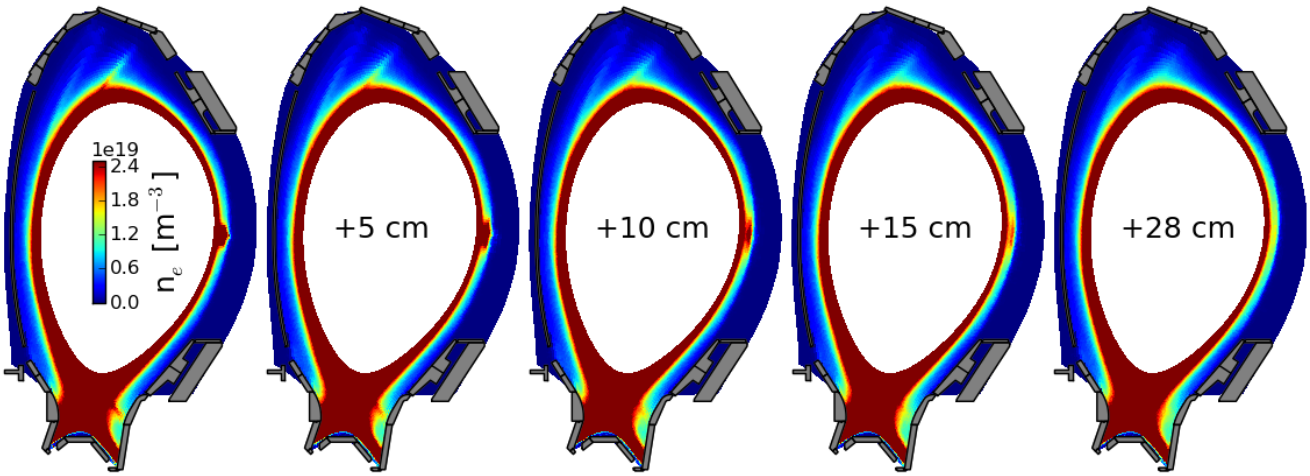

Figure 11. Variations of the 2D density profiles when radially shifting the outer mid-plane gas valve outward.

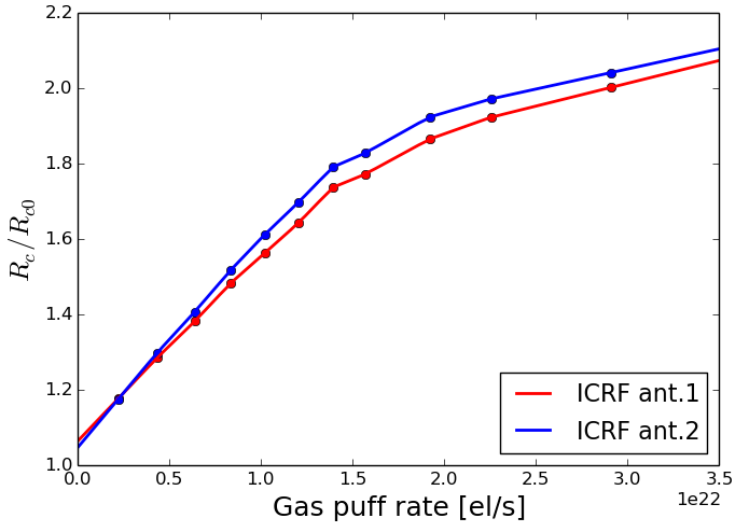

Figure 12. The simulated relative resistance as a function of gas puff rate for a typical H-mode discharge (#31269).